Synthesis, Characterization, and SERS Functionalization of Hollow Gold Nanoparticles

Debra Van Egeren

under the direction of
Dr. Amit Singh and Prof. Mansoor Amiji
Northeastern University

Research Science Institute
July 26, 2011

Abstract

Hollow gold nanoparticles formed by galvanic replacement reactions have been extensively studied because their increased surface area and tunable optical properties have applications in catalysis, drug delivery, and photothermal cancer therapies. In this study, hollow gold nanoparticles (size 30-40 nm) were synthesized by transmetallation of tyrosine-reduced sacrificial solid silver nanospheres. UV-vis-NIR spectroscopy and TEM imaging of the samples taken during the reaction showed the formation of hollow, porous gold nanospheres. The nanoparticles were then successfully functionalized with PEG-thiol and 5-mercaptopentanenitrile (a Raman dye), and SERS imaging of live cells was attempted but not achieved. Dye-functionalized nanoparticles reduced MTT and interfered with cytotoxicity assay results.

Summary

Nanoparticles have many varied and exciting applications. In this study, hollow gold shells were produced by adding gold ions to a solution of solid silver nanospheres. The silver atoms donated their electrons to the gold ions, creating solid gold nanoshells after dissolution of the newly-formed silver ions. To view the nanoparticles in cells, a molecule with a unique molecular fingerprint was added to their surfaces. The synthesized nanoparticles were introduced in live tissue samples, but unfortunately could not be viewed inside the cells. Nanoparticles that can be located in living systems may be used for tracking nanoshell-based drug delivery systems, or may be modified to image live biological systems.

1 Introduction

Metal nanoparticles (NPs) have several promising applications in biology, chemistry, and medicine [1, 2]. Their synthesis and properties have been extensively studied to design functional particles that catalyze reactions, carry drugs, and thermally destroy malignant cells [3, 4, 5]. Gold nanoparticles are unique in that they can be used for the imaging of live cells, eliminating the need for radioactive or fluorescent labels with surface-enhanced Raman spectroscopy [6]. Noble metals are used to enhance the range and accuracy of cell imaging beyond the limits of traditional Raman spectroscopy, and may be functionalized with small molecules or peptides to target specific cells, track nanoparticle localization in real-time, or gather more information about the intracellular environment [7, 8, 9, 10]. In the present study, gold nanoparticles are synthesized, examined, and tagged with a Raman dye to study their localization in live tissue samples.

1.1 Hollow Gold Nanoparticle Synthesis

Gold nanoparticles can be produced in a variety of ways [6, 11, 12]. One method of obtaining hollow gold nanospheres, described in Shukla *et al.* [6], employs a galvanic replacement mechanism. In this procedure sacrificial solid silver nanospheres are first synthesized and purified to remove any excess reducing agent. Au^{3+} ions are then added to the silver nanoparticle solution, often as chloroauric acid, $HAuCl_4$. The standard reduction potential of the $AuCl_4^-/Au$ pair (.99 V) is higher than that of the Ag^+/Ag pair (.80 V), so the silver atoms reduce the gold ions, creating a layer of solid elemental gold on the surface of the silver nanoparticles [6]. The silver atoms are oxidized by the gold ions, and dissolve into the solution as free Ag^+ cations [6]. This transmetallation reaction is employed and characterized in this study.

1.2 Raman Spectroscopy Basics

Raman spectroscopy provides a non-invasive, non-destructive way to examine the chemical composition of a wide variety of samples. This technique measures Raman scattering, a phenomenon involving the inelastic collision of a photon and a molecule. In contrast to Rayleigh scattering, an elastic scattering process, the photon donates or receives energy from the molecule it collides with [8]. The amount of energy exchanged between the particles depends on the vibrational energy states of the molecule. Since vibrational energy is quantized, only discrete quantities of energy may be given or received from the photon [8, 13]. Each molecule has unique set of allowed Raman energy transitions, so the pattern of Raman-scattered photons creates a fingerprint that is diagnostic of specific molecules. Raman spectroscopy measures the differences in energy between incident photons of monochromatic light emitted by a laser and the photons collected by a detector in the spectrophotometer after scattering off the sample. However, the intensity of Raman-scattered light is typically very low at laser intensities that are not damaging to live cells, and consequently, Raman spectra of biological samples are often difficult to obtain [8].

1.3 Surface-Enhanced Raman Spectroscopy

Surface-enhanced Raman spectroscopy (SERS) employs rough transition metal surfaces, usually nanoparticles, to increase the intensity of the Raman-scattered light [13]. This amplification is due to either the direct enhancement of the electromagnetic field detected by Raman spectroscopy or electronic interactions between the metal nanostructure (the SERS substrate) and the surrounding molecules [8]. The electromagnetic field enhancement crucial to SERS relies on localized surface plasmon resonance (LSPR) of the metal nanoparticles [14]. LSPR is the light-induced oscillation of charged particles within nanoscale metal structures. Energy from frequencies of light that correspond to the intrinsic resonant frequency of

the nanoparticle (the plasmon frequency) is transferred to the metal, causing harmonic oscillation of its electrons [14]. This absorbance of light by the nanoparticles is the origin of the color characteristic of many colloidal noble metal solutions, as the plasmon frequency generally lies in the visible region of the electromagnetic spectrum [15]. This oscillation causes the particles to increase the intensity of both the incident electromagnetic frequency (light from the laser) and Raman-shifted electromagnetic frequency (light scattered from the molecule) [14]. However, the electromagnetic waves must be at or near the intrinsic plasmon resonance frequency of the nanostructure to be enhanced by the nanoparticles [15].

1.4 SERS Substrates

Nanoparticles with different sizes, shapes, composition, and dissolved in different media are SERS-active at different wavelengths, because they have different plasmon resonance frequencies [14, 16]. Because different laser wavelengths are more appropriate for different samples, the plasmon frequencies of SERS nanoparticles must be carefully tuned to match specific wavelengths of light. For imaging of biological systems, laser wavelengths in the red or near-infrared (NIR) regions are often optimal because water and hemoglobin have the lowest extinction coefficient at these wavelengths [10]. Consequently, SERS at these wavelengths is better accomplished using gold rather than silver nanoparticles, because gold nanoparticles tend to absorb at red or NIR wavelengths [10]. However, as the intensity of Raman scattered light increases with the frequency of the incident light, blue or yellow lasers are often employed to increase the SERS sensitivity [17]. Gold nanoparticles are the most popular choice for imaging of live systems, due to their lack of cytotoxicity, strong SERS capabilities, stability, and ability to enter cells [8, 9, 13, 18].

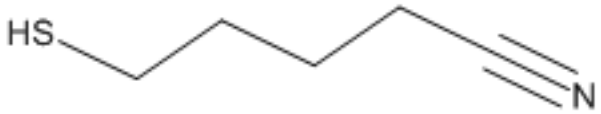

Figure 1: Structure of 5-mercaptopentanenitrile, the Raman dye used in this study. Note the presence of both nitrile and thiol groups in the molecule.

1.5 Functionalization of SERS Nanoparticles

Conjugation of specialized molecules to the surface of nanoparticles used for SERS is essential to the proper distribution and function of the nanoparticles. Conjugation of a polymer such as polyethylene glycol (PEG) on the surface of the nanoparticles improves their dispersion, biocompatibility, and the stabililty of their optical properties [10]. A dye or molecular probe can also be added to the nanoparticle surface to generate a clear and unique set of SERS features that may change according to the environment in which the nanoparticles are located [9]. Compounds with nitrile groups (C≡N) are particularly useful in SERS imaging of biological samples, because the nitrile functional group provides a sharp C≡N stretching mode at 2200–2300 cm^{-1} [19]. The cyano group is not naturally occuring, and biomolecules have few Raman features in the region 2200–2300 cm^{-1} that could interfere with the detection of the nitrile stretching mode [20]. The dye used in this study, 5-mercaptopentanenitrile (Figure 1), includes a nitrile group to provide a characteristic, identifiable peak in the *in vivo* SERS spectra and a thiol group (S–H) to allow the dye to conjugate to the nanoparticle surface.

This study examines the physical, optical, and biological properties of hollow gold nanoparticles. The hollow gold nanoparticles are also conjugated with a Raman reporter and introduced into live tissue samples to investigate their imaging capabilities.

2 Materials and Methods

2.1 Synthesis of Gold Nanoparticles

Hollow gold spherical nanoshells were synthesized through the sacrificial oxidation of silver by Au^{3+}, following the protocol described in Shukla *et al.* [6]. Solid silver nanospheres were synthesized through reduction of Ag^{+} by tyrosine under basic conditions. For this reaction, 1 mL of aqueous 10^{-2} M Ag_2SO_4 (Fisher Scientific), 10 mL of 10^{-3} M tyrosine (Acros Organics), and 10 mL aqueous KOH (10^{-2} M, Fisher) were added to 79 mL of deionized (DI) water. This solution was boiled until the solution turned deep yellow, about 5 minutes after boiling began. The solution of silver nanoparticles was then cooled and purified through dialysis in Sigma-Aldrich high retention seamless cellulose dialysis tubing (MW 11035) against DI water overnight.

The purified silver nanoparticles were then dialyzed against 2.2 L of 5×10^{-5} M aqueous $HAuCl_4$ solution (Sigma) until the solution turned grayish-yellow and the dialysis bag was covered with purple gold deposits. To monitor the progress of the reaction, 1.3 mL aliquots of the solution were taken at 15 min, 30 min, and 45 min after the beginning of the reaction, and again at 1, 2, 3, 5, and 7 hours after the reaction started for analysis with UV-visible-NIR (UV-vis-NIR) spectroscopy and transmission electron microscopy. The nanoparticles were removed from the dialysis bag after 7 hours and then functionalized.

2.1.1 UV-vis-NIR Characterization of Nanoparticles

UV-vis-NIR spectra were taken of samples of undialyzed and dialyzed silver nanoparticles and of samples taken during the course of the transmetallation reaction. The optical density from 200 nm to 1100 nm of each sample was taken with an Agilent 8453 UV-Visible Spectrophotometer in a quartz cuvette after arbitrary dilution of each sample.

2.1.2 Transmission Electron Microscopy of Nanoparticles

Dialyzed silver nanoparticle solution and samples taken at 1, 2, 3, 5, and 7 hours after the beginning of the transmetallation reaction were dried on copper electron microscopy grids (Electron Microscopy Sciences, 200 square mesh). Images of the grids were taken using a JEOL JEM-1010 transmission electron microscope (TEM) to observe morphological changes as the reaction progressed.

2.2 Functionalization of Au Nanoparticles with Polyethylene Glycol (PEG)

Previously synthesized borohydride-reduced, citrate-reduced, and hollow silver-reduced gold nanoparticles were PEGylated. A 500 μM aqueous solution of PEG-thiol (Laysan Bio, Inc) was made by dissolving 1.6 mg of PEG-thiol (molecular weight 2000 g/mol) in 1 mL of DI water. 100 μL of this solution was then added to 1.5 mL each of the gold nanoparticle solutions, and the resulting solutions were incubated at room temperature for 1 hour, with constant agitation. The solutions were then centrifuged at 16060g with a Fisher Scientific accuSpin Micro R Benchtop Centrifuge at 20°C for 20 minutes. The supernatant was discarded to remove excess PEG, and the pellets were resuspended in 1 ml portions of 1X phosphate-buffered saline (PBS, Gibco). Samples coated with PEG were stored in PBS at 4°C after synthesis. Surface-enhanced Raman spectra of the samples were then obtained.

2.3 Raman Spectroscopy of PEGylated Au Nanoparticles

Using a micropipette, 5 μL of each PEGylated nanoparticle solution was placed on a CaF_2 plate (Sigma) and allowed to dry. The Raman spectrum of each sample was taken from one focal point with a WITec CRM 200 confocal Raman microscope using a 488 nm solid-state laser under 100X magnification.

2.4 SERS Nanoprobe Preparation

2.4.1 Deprotection of (4-cyanobutyl)thioacetate

In a two-necked, round-bottom flask, 1 mL of (4-cyanobutyl)thioacetate, as purchased from Sigma, was dissolved in 10 mL of ethanol (Acros). 2.5 mL of 7 M aqueous NaOH (Fisher) was added dropwise to the flask with continuous stirring. The flask was then heated and refluxed for 2 hours. The mixture was degassed and placed under an inert nitrogen atmosphere. 6 mL of 2 M degassed hydrochloric acid (Fisher) was then added to the mixture, and the resulting solution was placed in a separatory funnel. 20 mL of diethyl ether (Acros) and 10 mL of DI water were then added to the mixture, and the resulting aqueous phase discarded. The remaining organic phase was washed once with 10 mL of degassed water and allowed to dry over sodium sulfate (Merck). The final mixture contained 5-mercaptopentanenitrile in diethyl ether.

2.4.2 Functionalization of Gold Nanoparticles

Hollow and citrate-reduced solid gold nanoparticle samples were functionalized with 5-mercaptopentanenitrile, a cyano-containing Raman reporter, and PEG-thiol (MW 2000). 500 μL of 5-mercaptopentanenitrile in diethyl ether was added to 1 mL each of the aqueous nanoparticle solutions. The samples were then vigorously shaken and sonicated in a water bath for 10 minutes to break up nanoparticle aggregates. The samples were vacuum-dried at room temperature until the organic phase evident at the top of the samples disappeared. 200 μL of PEG-thiol solution prepared from 1.6 grams of dry PEG-thiol and 1 mL of DI water was then added to each nanoparticle solution. The samples were sonicated again and incubated at room temperature for 1 hour, then centrifuged with a Fisher Scientific accuSpin Micro R Benchtop Centrifuge at 16060g for 30 minutes at 25°C. After vacuum-drying overnight, the nanoparticle solutions were centrifuged again at 16060g for 30 minutes at

25°C, and the supernatant was discarded. The pellet was then resuspended in 500 mL of 1X PBS. The Raman spectra of these particles were measured using the procedure described in Section 2.3.

2.5 Determination of PEGylated Dye-Functionalized Au and Ag Nanoshell Cytotoxicity

2.5.1 Growth of Cell Culture and Incubation with Nanoparticles

Panc1 cells were grown in a RPMI-1640 (Cellgro) complete medium containing 10% fetal bovine serum (Gemini Bioproducts) and 1% penicillin-streptomycin-amphotericin B antibiotic mixture at 37°C in 5% CO_2. The cells were counted with a hemocytometer, and a 96-well plate was prepared with 3000 cells per well. 25%, 50%, and 75% nanoparticle solutions were made through dilution of dye-functionalized PEG-conjugated hollow gold nanoparticles and dye-functionalized PEG-conjugated solid silver nanoparticles with complete medium. 200 μL of each solution was added to 7 wells containing cell cultures. 14 wells were incubated with only complete medium as controls (100% cell viability). The 96-well plate was incubated for 24 hours at 37°C in 5% CO_2 and was assessed for cell viability with an MTT assay.

2.5.2 MTT Assays

After incubation with nanoparticle solutions, culture medium from the wells was removed and discarded. 100 μL of aqueous 3-(4,5-dimethylthiazol-2-yl)-2,5-diphenyltetrazolium bromide (MTT, Sigma) solution (1 mg dry MTT per mL water) was added to each well. The cells were incubated in MTT solution for 3 hours at 37°C. 150 μL of dimethyl sulfoxide (DMSO, Fisher) was added to each well to dissolve any formazan crystals, and the optical density of each well at 570 nm was measured with a BioTek Synergy HT Microplate Reader to determine the amount of formazan in each well.

The assay was repeated with only nanoparticle and dye solutions. Eight 50 μL aliquots each of DI water, 5-mercaptopentanenitrile in diethyl ether, gold nanoparticles with PEG, and gold nanoparticles with dye and PEG were added to a 96-well plate. 100 μL of MTT solution (1 mg/mL) was added to each well. The wells were shielded from light and incubated at room temperature for 3 hours. 150 μL of DMSO was added to each well, and the absorbance at 570 nm of each well was then measured. The sample with DI water in place of nanoparticles or dye was used as a blank.

2.6 Surface-Enhanced Raman Microspectroscopy of Cell Cultures

Cell culture samples were incubated for 3 hours with 50 μL, 100 μL, and 200 μL portions of undiluted PEGylated and dye-functionalized hollow gold nanosphere solutions, and imaged with a Raman confocal microscope at 488 nm. Spectra were processed using Vertex Component Analysis (VCA) to determine the intracellular distribution of organic molecules and dyed nanoparticles.

3 Results and Discussion

3.1 Gold Transmetallation Reaction Progress

The samples that were measured with UV-vis-NIR absorbance spectroscopy were not diluted to the same concentration, making quantitative and qualitative comparison among the samples difficult. Quantitative comparison among the peaks of individual spectra, however, provides more useful data. Silver nanoparticles absorb at wavelengths near 400 nm, while gold nanoshells absorb light at higher wavelengths [6]. The ratio of absorbance at 800 nm to the absorbance at 407 nm for each sample measured is shown in Figure 2. The ratio increases monotonically as the reaction progresses, indicating an increase in the amount of gold rela-

tive to the amount of silver in the nanoparticles. This is consistent with the predicted result of the transmetallation reaction; the gold is reduced, forming a shell on the silver surface, leading to a plasmon absorbance peak in the NIR range, while the silver dissolves away as Ag^+, causing a reduction in intensity of the silver absorption peak at about 400 nm.

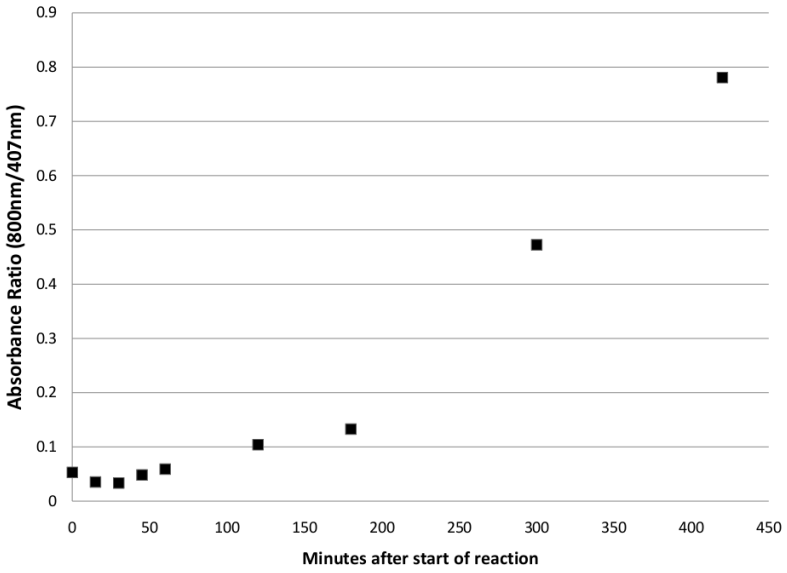

Figure 2: Absorbance ratio of nanoparticle samples taken at 0, 15, 30, 45, 60, 120, 180, 300, and 420 minutes after the start of transmetallation.

The absorbance spectrum for the last time point (420 minutes, the time at which the reaction was stopped) is shown in Figure 3. The gold absorption peak at about 800 nm is clearly visible, although the sample still has a small feature at 450 nm, indicating the persistence of silver in the nanoparticles. The nanoparticles are still SERS-active at 488 nm, the wavelength of light used in the Raman measurements in Section 2.3.

TEM images of the nanoparticles at various time points during the transmetallation reaction were taken, and shown in Figure 4. During the earlier stages of reaction, distinct regions of gold deposition are evident and appear as dark circular spots on some of the

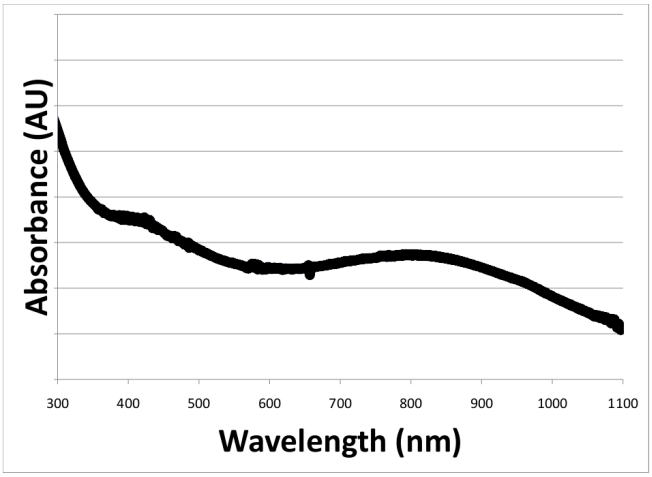

Figure 3: UV-vis-NIR absorbance spectrum for the finished gold nanoparticles (time = 420 min) from 300 to 1100 nm

nanoparticles (Figures 4B and 4C, circled areas). These reaction initiation sites often occur specifically at small defects in the silver crystal structure on the nanoparticle surface [6]. As more gold is reduced, the structures become more hollow and porous, eventually resulting in the nanoshells seen in Figure 4F (circled area).

3.2 Functionalized Nanoparticle Production

The SERS spectra of PEGylated borohydride-reduced, citrate-reduced, and silver-reduced gold nanoparticles are shown in Figure 5. Most of the peaks below 1500 cm^{-1} cannot be assigned to specific groups, as peaks in this region are due to more complex vibrations of larger portions of the molecule and are dependant on the entire molecular structure [19]. However, the peaks for wavenumbers 500–1500 cm^{-1} appear at similar positions in all of the samples tested, indicating the predominance of the same molecule (likely PEG) at the surface of each nanoparticle type tested. The non-specific increase in the scattered light intensity of the borohydride-reduced solid gold nanoparticle sample was due to unintended fluorescence

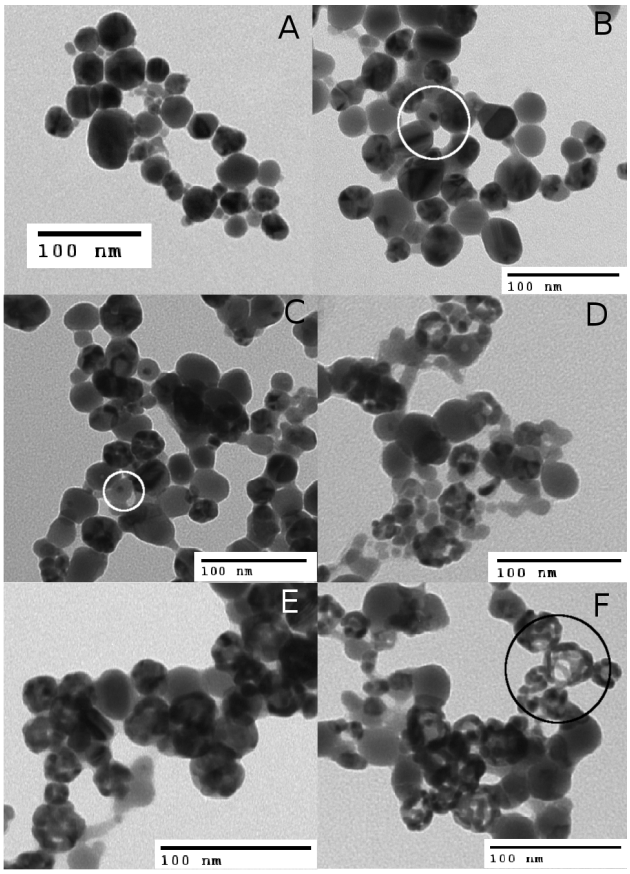

Figure 4: TEM images of dialyzed silver nanoparticles (A) and nanoparticles taken at 1 (B), 2 (C), 3 (D), 5 (E), and 7 hours (F) after the beginning of the transmetallation reaction

of PEG under the Raman measurement conditions.

Raman spectroscopy results from the PEG- and dye-conjugated nanoparticles outside of cells were obtained (Figure 6). Evident in spectra from each of the samples is a sharp peak around 2255 cm^{-1} not present in the spectra of samples only functionalized with PEG. This peak corresponds to the stretching of the cyano functional group in 5-mercaptopentanenitrile, and its intensity will be used to create a Raman map of the tissue samples. The dye has conjugated to the nanoparticle surface and is easily detectable with SERS.

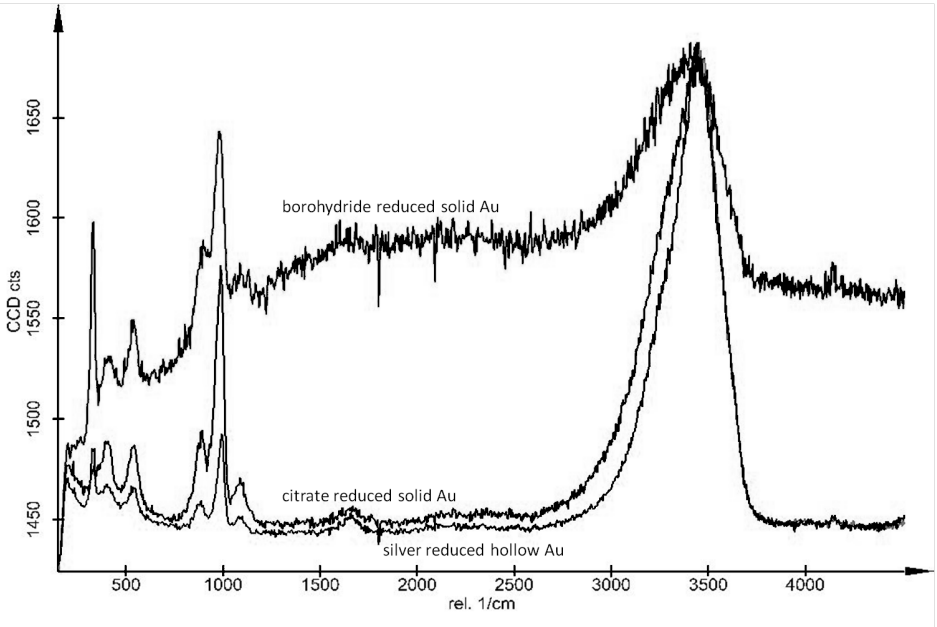

Figure 5: SERS spectra of borohydride-reduced, citrate-reduced, and silver-reduced gold nanoparticles. Note the similarity of the fingerprint peaks for wavenumbers 500–1500 $cm^{-}1$.

3.3 Cytotoxicity of PEGylated and Dye-Functionalized Nanoparticles

The optical densities (OD) at 570 nm for wells treated with the same nanoparticle concentration were averaged and are shown in Table 1. The average OD for the wells without added nanoparticles was defined as 100% cell viability and is not shown. All of the wells treated with nanoparticle solutions show more purple formazan production than the untreated wells. These results seem to indicate that more cells are alive in the wells incubated with nanoparticles, because the reduction of MTT to formazan is thought to be caused by metabolic activity in live cells [21]. However, it is not likely that silver or gold nanoparticles are causing such a dramatic increase in cell growth or metabolism, so other causes of MTT reduction were investigated.

Wells containing MTT were incubated with dyed gold nanoparticles, PEGylated gold nanoparticles, and Raman dye alone. Their average optical densities are shown in Table 2.

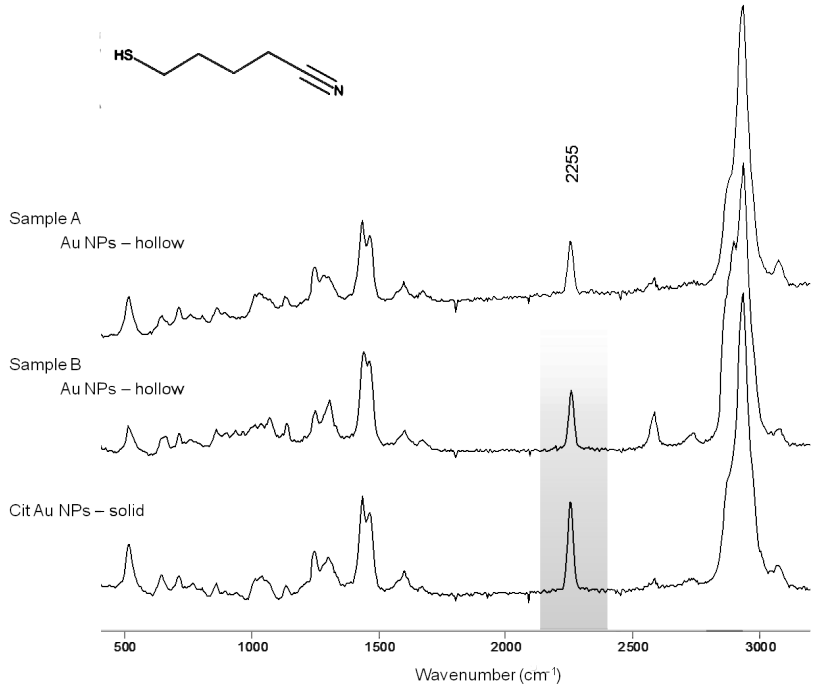

Figure 6: SERS spectra of silver-reduced and citrate-reduced nanoparticles functionalized with PEG and 5-mercaptopentanenitrile

Gold nanoparticles functionalized with 5-mercaptopentanenitrile reduced MTT. The MTT assay results shown in Table 1 can not be reliably used to assess the biological effects of dye-functionalized nanoparticles, because the reduction capabilities of the nanoparticles themselves interferes with the assay.

3.4 Surface-Enhanced Raman Imaging of Live Cells

Figure 7 shows the Raman microspectroscopy image, with brighter areas showing increased C–H stretching mode intensity, indicative of the distribution of organic molecules in the sample. The outline of the cell is distinct and the nucleus is evident as a bright circle in the cell, because DNA rich in C–H is densely packed in the nucleus. The same set of spectral data were examined for the distribution of nitrile groups, with brighter areas indicating increased C≡N stretching mode intensity, is shown in Figure 8. The nitrile stretching intensity is

% NP solution	Absolute Avg OD	$\frac{OD_{570,\text{ with NPs}}}{OD_{570,\text{ control}}}$
75% Ag	2.547	3.431
50% Ag	0.905	1.220
25% Ag	0.771	1.038
75% Au	1.394	1.878
50% Au	0.933	1.257
25% Au	0.757	1.020

Table 1: Relative cell viability after 24 hours of incubation with functionalized nanoparticle solutions

Sample	Average OD
PEGylated NPs	0.080
Dyed NPs	0.703
Dye	0.411

Table 2: Average optical density of wells incubated with MTT and gold nanoparticles or dye. The average blank OD has been subtracted from each value.

approximately equal in all regions of the sample. It is unlikely that the nanoparticles were evenly distributed throughout the sample, because gold nanoparticles do not usually enter the nucleus [9]. These results may be due to an insufficient concentration of nanoparticles during the incubation period or unfavorable imaging conditions.

4 Conclusion

Hollow gold nanoparticles were synthesized by galvanic replacement reaction with sacrificial silver nanospheres. As the reaction progressed, silver was oxidized and dissolved away, and elemental gold deposits formed a porous shell. The reaction began at distinct sites on the silver nanoparticle surface and resulted in the formation of a hollow nanostructure suitable for functionalization with PEG and a Raman dye. UV-vis-NIR spectroscopy indicated that the synthesized hollow gold nanoparticles are SERS-active at 488 nm, the chosen laser wavelength for the Raman studies. Both PEG and 5-mercaptopentanenitrile were conjugated to the nanoparticle surface successfully, and were detectable with SERS. However, the dye-functionalized nanoparticles failed to generate useful Raman tracking data in live cells. Gold nanoparticles functionalized with 5-mercaptopentanenitrile reduce MTT, making assessment

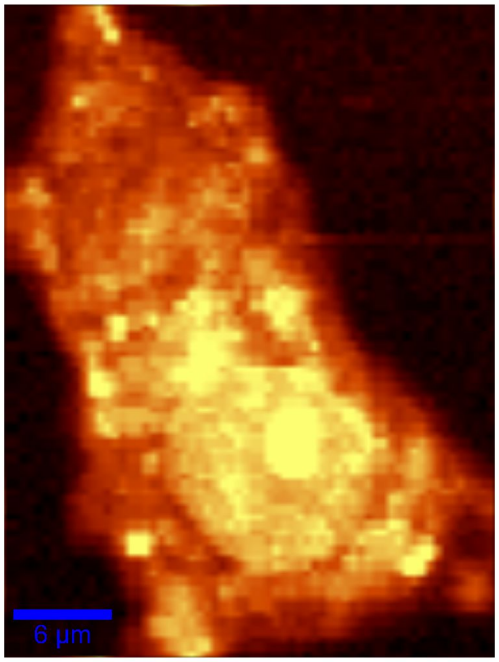

Figure 7: Raman image of the C–H stretching mode intensity in a Panc1 cell

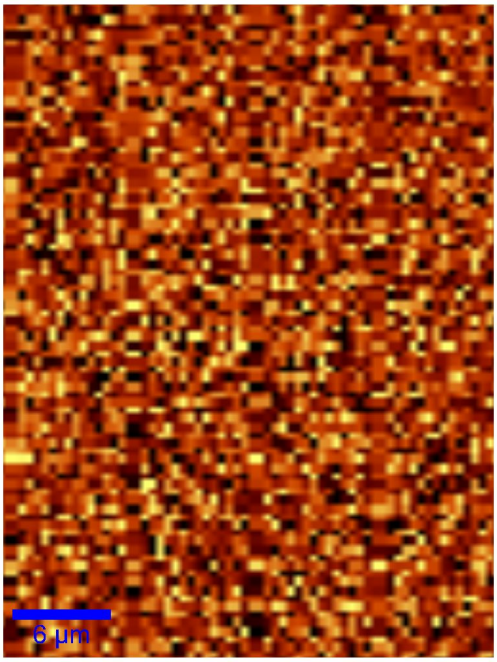

Figure 8: Raman image of the C≡N stretching mode intensity in the same cell

of dye-functionalized nanoparticle cytotoxicity with an MTT assay difficult.

5 Acknowledgments

I would like to thank Prof. Mansoor Amiji and Dr. Amit Singh for the time, effort, and resources they sacrificed to allow this project to be successfully completed, as well as Dr. Tatyana Chernenko for her assistance in obtaining the Raman images. I would also like to acknowledge my tutor, Annie Ouyang, for her support and suggestions throughout the summer, as well as the rest of the RSI staff. I am very grateful for all the sponsors who have donated resources to RSI, especially Biogen Idec and Mr. Sean Kanuck. Finally, I thank the Center for Excellence in Education, as well as MIT, for sponsoring and hosting this program and making my stay and research here possible.

References

[1] J. Chen, D. Wang, J. Xi, L. Au, A. Siekkinen, A. Warsen, Z. Li, H. Zhang, Y. Xia, X. Li. Immuno gold nanocages with tailored optical properties for targeted photothermal destruction of cancer cells. *Nano Letters* 7 (2007), no. 5, 1318–1322.

[2] G. Wu, A. Mikhailovsky, H. A. Khant, C. Fu, W. Chiu, J. A. Zasadzinski. Remotely triggered liposome release by near-infrared light absorbption via hollow gold nanoshells. *Journal of the American Chemical Society* 130 (2008), no. 26, 8175–8177.

[3] R. Kumar, A. N. Maitra, P. K. Patanjali, P. Sharma. Hollow gold nanoparticles encapsulating horseradish perioxidase. *Biomaterials* 26 (2005), 6743–6753.

[4] J. You, G. Zhang, C. Li. Exceptionally high payload of doxorubicin in hollow gold nanospheres for near-infrared light-triggered drug release. *ACS Nano* 4 (2010), no. 2, 1033–1041.

[5] M. P. Melancon, W. Lu, Z. Yang, R. Zhang, Z. Cheng, A. M. Elliot, J. Stafford, T. Olson, J. Z. Zhang, C. Li. *In vitro* and *in vivo* targeting of hollow gold nanoshells directed at epidermal growth factor receptor for photothermal ablation therapy. *Molecular Cancer Therapeutics* 7 (2008), no. 6, 1730–1739.

[6] S. Shukla, A. Priscilla, M. Banerjee, R. R. Bhonde, J. Ghatak, P. V. Satyam, M. Sastry. Porous gold nanospheres by controlled transmetalation reaction: a novel material for application in cell imaging. *Chemistry of Materials* 17 (2005), no. 20, 5000–5005.

[7] S. Schlücker. SERS microscopy: nanoparticle probes and biomedical applications. *ChemPhysChem* 10 (2009), no. 9–10, 1344–1354.

[8] J. Kneipp, H. Kneipp, B. Wittig, K. Kneipp. Novel optical nanosensors for probing and imaging live cells. *Nanomedicine: Nanotechnology, Biology and Medicine* 6 (2010), no. 2, 214–216.

[9] M. A. Ochsenkühn, P. R. T. Jess, H. Stoquer, K. Dholakia, C. J. Campbell. Nanoshells for surface-enhanced Raman spectroscopy in eukaryotic cells: cellular response and sensor development. *ACS Nano* 3 (2009), no. 11, 3613–3621.

[10] X. Qian, X. Peng, D. O. Ansari, Q. Yin-Goen, G. Z. Chen, D. M. Shin, L. Yang, A. N. Young, M. D. Wang, S. Nie. *In vivo* tumor targeting and spectroscopic detection with surface-enhanced Raman nanoparticle tags. *Nature Biotechnology* 26 (2008), no. 1, 83–90.

[11] M. Daniel, D. Astruc. Gold nanoparticles: assembly, supramolecular chemistry, quantum-size-related properties, and applications toward biology, catalysis, and nanotechnology. *Chemical Reviews* 104 (2004), no. 1, 293–346.

[12] N. R. Jana, L. Gearheart, C. J. Murphy. Seeding growth for size control of 5–40 nm diameter gold nanoparticles. *Langmuir* 17 (2001), no. 22, 6782–6786.

[13] W. Xie, L. Su, A. Shen, A. Materny, J. Hu. Application of surface-enhanced Raman scattering in cell analysis. *Journal of Raman Spectroscopy* 42 (2011), no. 6, 1248–1254.

[14] K. A. Willets, R. P. Van Duyne. Localized surface plasmon resonance spectroscopy and sensing. *Annual Review of Physical Chemistry* 58 (2007), 267–297.

[15] A. M. Schwartzberg, T. Y. Olson, C. E. Talley, J. Z. Zhang. Synthesis, characterization, and tunable optical properties of hollow gold nanospheres. *Journal of Physical Chemistry B* 110 (2006), no. 40, 19935–19944.

[16] C. J. Murphy, A. M. Gole, J. W. Stone, P. N. Sisco, A. M. Alkilany, E. C. Goldsmith, S. C. Baxter. Gold nanoparticles in biology: beyond toxicity to cellular imaging. *Accounts of Chemical Research* 41 (2008), no. 12, 1721–1730.

[17] E. Smith, G. Dent. *Modern Raman Spectroscopy: a Practical Approach*. Wiley, Hoboken, NJ, (2005).

[18] H. Park, S. Lee, L. Chen, E. Lee, S. Shin, Y. Lee, S. Son, C. Oh, J. Song, S. Kang, J. Choo. SERS imaging of HER2-overexpressed MCF7 cells using antibody-conjugated gold nanorods. *Physical Chemistry Chemical Physics* 11 (2009), 7444–7449.

[19] D. W. Mayo, F. A. Miller, R. W. Hannah. *Course Notes on the Interpretation of Infrared and Raman Spectra*. Wiley, Hoboken, NJ (2003).

[20] B. A. Lindquist, K. E. Furse, S. A. Corcelli. Nitrile groups as vibrational probes of biomolecular structure and dynamics: an overview. *Physical Chemistry Chemical Physics* 11 (2009), no. 37, 8119–8132.

[21] Y. Liu, D. A. Peterson, H. Kimura, D. Schubert. Mechanism of cellular 3-(4,5-dimethylthiazol-2-yl)-2,5-diphenyltetrazolium bromide (MTT) reduction. *Journal of Neurochemistry* 69 (1997), no. 2, 581–593.